IEEE Access
Multidisciplinary | Rapid Review | Open Access Journal

Received December 13, 2020, accepted December 23, 2020, date of publication January 1, 2021, date of current version January 12, 2021.

Digital Object Identifier 10.1109/ACCESS.2020.3048717

Intent Inference of Ship Collision Avoidance Behavior Under Maritime Traffic Rules

YONGHOON CHO, (Graduate Student Member, IEEE), JONGHWI KIM, (Graduate Student Member, IEEE), AND JINWHAN KIM, (Member, IEEE)

Department of Mechanical Engineering, Korea Advanced Institute of Science and Technology, Daejeon 34141, South Korea

Corresponding author: Jinwhan Kim (jinwhan@kaist.ac.kr)

This research was supported by the 'Development of Autonomous Ship Technology (PMS4460, development of autonomous navigation system with intelligent route planning function)' funded by the Ministry of Oceans and Fisheries (MOF, Korea), and in part by the KAIST Institute.

ABSTRACT This paper proposes an algorithm to infer the maneuver intention of an obstacle ship and to check its compliance with the maritime traffic rules to avoid ship collision and ensure maritime traffic safety. A probabilistic graphical model is constructed to represent the relationship between motion observations of the obstacle ship and its hidden maneuver intention to comply with the traffic rules. The probabilistic belief of the ship's intention is modeled and quantified using probabilistic tools such as dynamic Bayesian networks. Three different intent inference models are formulated considering the different levels of observation configurations, and their calculation procedures are described. To demonstrate the feasibility of the proposed intent inference algorithm, Monte-Carlo simulations were conducted and the results are presented.

INDEX TERMS Intent inference, COLREGs, ship collision avoidance, dynamic Bayesian network.

I. INTRODUCTION

SHIPS navigating in open waters are obliged to comply with the international regulations for preventing collisions at sea (COLREGs), which correspond to the traffic laws of public roads [1]. The COLREGs, adopted by the international maritime organization (IMO), contain various rules for maritime traffic safety, such as the light and sound signals for communications and guidelines on vessel priority [2]–[4]. In particular, the regulations provide a conflict resolution procedure to resolve encounters between ships. However, not all ships strictly follow this procedure and the rules can sometimes be interpreted differently between the encountering ships, which may lead to dangerous situations [5]. Therefore, estimating the maneuver intention of the other ships at sea regarding their compliance to the maritime traffic rules is important and necessary to ensure safe ship navigation, especially for autonomous surface ships and conventional ships with automated collision avoidance systems. However, information regarding the maneuver intention is usually hidden and cannot be readily identified if not broadcasted or shared through communication channels. Therefore, it has to be estimated from the ship's trajectory, where the operator's maneuver intention has been reflected.

Much research for estimating maneuver intention has been performed in the field of intelligent aerial vehicles and air traffic management. There exist some similarities between aviation and maritime traffic systems. Unlike cars on roadways, aircraft and ships are operated in open space with no traffic infrastructure such as visible traffic lanes and signal lights. In the aviation domain, the flight intention is represented by trajectory change points (TCPs) which can be provided via automatic dependent surveillance-broadcast (ADS-B). However, considering the vulnerability of ADS-B to fake data injection and system failures, many studies have focused on predicting or estimating the aircraft intention using flight trajectory observations. In [6], the navigation intention was inferred from the given state of an aircraft in a horizontal-vertical-speed dimension, and the intention was evaluated by the likelihood function based on the estimation error of the tracking filter and the sensor noises in [7] and [8]. In [9], dynamic Bayesian networks (DBNs) were used for the joint target tracking, classification, and intent inference (JTCI) which is an extended version of the joint target tracking and classification (JTC).

Although there exist some similarities between the aviation and maritime traffic systems, there also exists a significant

The associate editor coordinating the review of this manuscript and approving it for publication was Yougan Chen.

difference between them, and as a result, the intent inference methods for aviation traffic management cannot be directly applied to maritime applications. The roles of an aircraft pilot and a ship's captain in air traffic or vessel traffic management systems are quite different. While the aircraft is constantly monitored and guided by air traffic controllers, the ship's captain holds the full responsibility of the operation. In other words, ships operate much more individually than aircraft. Most importantly, all the ships are required to comply with the maritime traffic rules, COLREGs, and therefore it is important to consider these maritime specific rules in estimating the ship's maneuver intention and predicting its potential evasive action. Little research on intent inference has been performed in the maritime domain compared to that in the aviation domain. The concept of intent-aware collision avoidance between surface vehicles was addressed in [10]. A propagation model to deal with the intention of other ships was proposed and it was applied in [11]–[13]. In [14], the Douglas-Peucker algorithm and the nonlinear velocity obstacle (NLVO) were used to predict the give-way vessel's intention; however, the study did not address the intention of the stand-on vessel. The existing rules are quantified using the case law to detect the other ship's rule violation [15]; however, it did not consider the effect of inherent uncertainty and measurement noise in quantifying the degree of rule violation. In fact, the amount of information for intent inference may vary depending on sensor/communication configurations, and the information provided by navigation sensors – such as automatic information system (AIS) and marine radar – is corrupted by measurement noise. These issues have not been sufficiently explored in the above-mentioned studies, and to the best of the authors' knowledge, none of the existing studies in the maritime domain has provided an explicit probabilistic model for intent inference.

This paper presents a novel approach for inferring the maneuver intention of a ship using its trajectory information with measurement uncertainty. To quantify the probability of compliance to the maritime traffic rules of an encountered obstacle ship, a graphical model is constructed based on the DBN combining graphical models for state-action-intention and measurement-state-action. The probability of rule compliance is defined as the belief of intention based on the proposed graphical model, and the procedure to factorize the belief into familiar probability distributions is newly proposed using various probabilistic techniques and tools. The procedure of modeling the probability distribution and calculating the belief is described considering the availability of trajectory observations and their uncertainty. The performance of the proposed method is demonstrated using Monte-Carlo-based ship traffic simulations, and the simulation results are discussed.

The remainder of this paper is organized as follows: Section II describes the problem formulation of the intent inference to predict the maneuver intention and the mathematical derivation to factorize and calculate the belief. Section III presents parametric and nonparametric modeling of the probability distribution. The results of the Monte-Carlo simulation are described in Section IV, and finally, the conclusions are presented in Section V.

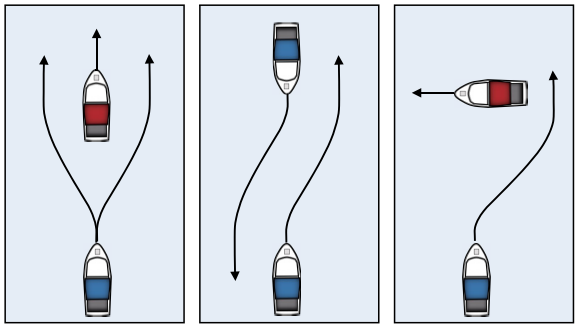

FIGURE 1. Illustrations of compliant maneuvers in vessel encounter situations defined in COLREGs: The blue ship takes a give-way maneuver, while the red ship takes a stand-on maneuver.

II. PROBLEM STATEMENT

A. MANEUVER INTENTION

The ship's maneuver intention is described as a latent reason or objective of the operator to manipulate the ship's rudder and engine telegraph. The operator controls the ship with various operational purposes and maneuver intentions. The intention to be addressed in this study is the intention of compliance of the vessels that are in sight of one another with the maritime traffic rules, COLREGs. The COLREG-compliant maneuvers of three encounter situations are depicted in Fig. 1. In each encounter situation, at least one give-way vessel exists, while the other has a stand-on duty so that they can avoid each other. The obligations of give-way and stand-on ships are described by rules 16 and 17 in the COLREGs as follows:

- **Rule 16 action by give-way vessel**: Every vessel which is directed to keep out of the way of another vessel shall, so far as possible, take early and substantial action to keep clear well.
- **Rule 17 action by stand-on vessel**-(a)(i): Where one of two vessels is to keep out of the way, the other shall keep her course and speed.

The ship's maneuver intention is assumed to be reflected on its trajectory. For example, when a ship with an obligation to give way alters its course to the port side, this behavior provides evidence of rule-violation. The elements of the intention's sample space $\mathcal{I} = \{\mathcal{C}, \mathcal{V}\}$ are assumed to be mutually exclusive, which means that compliant and non-compliant actions cannot be performed at the same time.

B. GRAPHICAL MODEL

The proposed graphical model based on a DBN for inferring the intentions of ship maneuvering is shown in Fig. 2. The DBN consists of four variables: $\mathbf{x}$, $\mathbf{u}$, I, and $\mathbf{z}$, which represent the state, action, intention, and measurement, respectively.

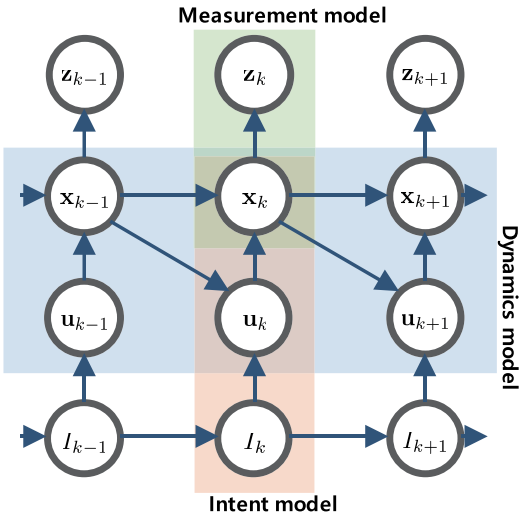

FIGURE 2. Dynamic Bayesian network for intent inference of ship maneuvering: The graphical model is constructed by merging the dynamics model (blue box), intent model (orange box), and measurement model (green box). x, u, z and *I* represent the state, action, measurement, and intention, respectively. The subscript *k* represents a time step. The horizontal direction represents the time axis.

The intention is denoted by I, which is defined as an element of set $\mathcal{I}$, and the subscript involving k is the index of the time step. The maneuver intentions create actions, and the actions evolve into the states. This procedure is described in Fig. 2 with the state, action, and intention nodes along the vertical axis, which is called the intent model. The change of intention over time is shown along the horizontal axis, which is called the intent transition model. The graphical model is constructed by combining the intent model and the intent transition model in the form of HMMs (hidden Markov models) [16], which consists of the evolution of the state, measurement, and action.

C. OBSERVATION CONFIGURATIONS

To infer the intention of the obstacle ship, a set of intent-related information is gathered, and its time history is accumulated. The amount and quality of information for inferring the intention of the obstacle ship may vary depending on the sensing and communication capabilities and operational settings. In this study, we consider the following three cases of information availability and show how the performance of intent inference changes with the information availability.

Here, the measurement $\mathbf{z}$ represents the range and bearing data (generally represented by a range and bearing) of the encountering ships observed from the own ship. The state $\mathbf{x}$ represents the position and heading data of the obstacle ship.

- **Case 1**: States ($\mathbf{x}$), action ($\mathbf{u}$), and measurements ($\mathbf{z}$) are available.
- **Case 2**: Only states ($\mathbf{x}$) are available. (e.g., AIS data)
- **Case 3**: Only measurements ($\mathbf{z}$) are available. (e.g., marine radar measurements)

The action $\mathbf{u}$ is the control input data of the obstacle ship that changes the state. Case 1 is the ideal case in which all the information is obtained without noise. Cases 2 and 3 are more realistic and practical cases assuming that the information is corrupted by measurement noise. In the practical scenario of Case 2, the AIS can provide the state information including the other ships' speed and course. Also, the onboard sensors such as the marine radar can measure the other ships' relative range and bearing in Case 3.

D. MATHEMATICAL MODELS

Here, the mathematical formulation for quantifying the intention and the resulting models are described. The value of the quantified intention defined as the belief of intention $bel(I)$ is calculated by probabilistic approaches such as the Bayes' rule and d-separation.

1) $bel(I_k)$ FOR CASE 1

The belief of intention can be represented as the probability of intention conditioned on the time history of all the information except for the intention itself and it is expressed as follows:

$$bel(I_k) = p(I_k|\mathbf{u}_{1:k}, \mathbf{x}_{0:k}, \mathbf{z}_{1:k}), \tag{1}$$

where the subscript $k_1 : k_2$ represents the time history from k_1 to k_2. According to the d-separation rule, I_k is conditionally independent of $\mathbf{x}_k$ and $\mathbf{z}_{1:k}$ given $\mathbf{u}_{1:k}$ and $\mathbf{x}_{0:k-1}$ from the graphical model in Fig. 2. Therefore, $bel(I_k)$ is simplified as

$$bel(I_k) = p(I_k|\mathbf{u}_{1:k}, \mathbf{x}_{0:k-1}). \tag{2}$$

This belief function is represented in a recursive form as

$$\begin{aligned} &p(I_k|\mathbf{u}_{1:k}, \mathbf{x}_{0:k-1}) \\ &= \eta_k p(\mathbf{u}_k|I_k, \mathbf{x}_{k-1}) \sum_{I_{k-1}} p(I_k|I_{k-1}) p(I_{k-1}|\mathbf{u}_{1:k-1}, \mathbf{x}_{0:k-2}) \\ &= \eta_k p(\mathbf{u}_k|I_k, \mathbf{x}_{k-1}) \sum_{I_{k-1}} p(I_k|I_{k-1}) bel(I_{k-1}), \end{aligned} \tag{3}$$

where $\eta_k = 1/p(\mathbf{u}_k|\mathbf{x}_{0:k-1}, \mathbf{u}_{1:k-1})$ is the normalizer. For more detail see Appendix A. The belief is separated into the intention-reflected action probability $p(\mathbf{u}_k|I_k, \mathbf{x}_{k-1})$, the intent transition probability $p(I_k|I_{k-1})$, and the prior belief function $bel(I_{k-1})$.

2) $bel(I_k)$ FOR CASE 2

If only the state information is given, the belief of intention can be represented as

$$bel(I_k) = p(I_k|\mathbf{x}_{0:k}). \tag{4}$$

The belief function is represented in a recursive form as before:

$$\begin{aligned} &p(I_k|\mathbf{x}_{0:k}) \\ &= \eta_k \int_{\mathbf{u}_k} p(\mathbf{x}_k|\mathbf{u}_k, \mathbf{x}_{k-1}) p(\mathbf{u}_k|I_k, \mathbf{x}_{k-1}) \sum_{I_{k-1}} p(I_k|I_{k-1}) \end{aligned}$$

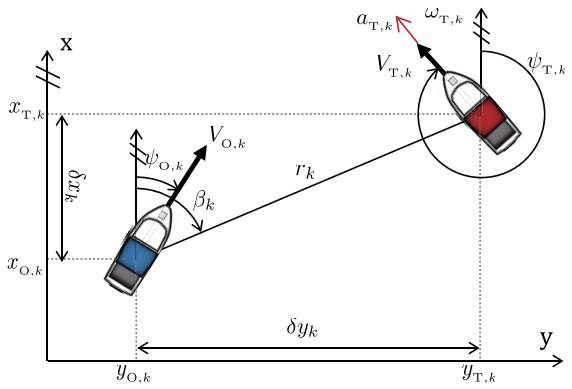

FIGURE 3. A graphical representation of the coordinates between the own ship and obstacle ship at time step k.

$$
\begin{aligned}
&p(I_{k-1}|\mathbf{x}_{0:k-1})d\mathbf{u}_k \\
&= \eta_k \int_{\mathbf{u}_k} p(\mathbf{x}_k|\mathbf{u}_k, \mathbf{x}_{k-1}) p(\mathbf{u}_k|I_k, \mathbf{x}_{k-1}) \sum_{I_{k-1}} p(I_k|I_{k-1}) \\
&\quad bel(I_{k-1})d\mathbf{u}_k . \qquad (5)
\end{aligned}
$$

Compared with (3), the state transition probability $p(\mathbf{x}_k|\mathbf{u}_k, \mathbf{x}_{k-1})$ is included because the action information is not directly given. Details of the derivation are presented in Appendix B.

3) $bel(I_k)$ FOR CASE 3

Finally, if only the measurement information is provided, the belief of intention can be represented as

$$bel(I_k) = p(I_k|\mathbf{z}_{1:k}). \qquad (6)$$

The method for recursive calculation of the belief slightly differs from the previous two calculation methods. The belief can be represented by the marginalization of the joint probability of state and intention at the current time step as follows:

$$p(I_k|\mathbf{z}_{1:k}) = \int_{\mathbf{x}_k} p(\mathbf{x}_k, I_k|\mathbf{z}_{1:k}) d\mathbf{x}_k . \qquad (7)$$

The joint probability is calculated recursively as

$$
\begin{aligned}
&p(\mathbf{x}_k, I_k|\mathbf{z}_{1:k}) \\
&= \eta_k p(\mathbf{z}_k|\mathbf{x}_k) \iint_{\mathbf{x}_{k-1}, \mathbf{u}_k} p(\mathbf{x}_k|\mathbf{u}_k, \mathbf{x}_{k-1}) p(\mathbf{u}_k|\mathbf{x}_{k-1}, I_k) \\
&\quad \sum_{I_{k-1}} p(I_k|I_{k-1}) p(\mathbf{x}_{k-1}, I_{k-1}|\mathbf{z}_{1:k-1}) d\mathbf{u}_k d\mathbf{x}_{k-1} . \qquad (8)
\end{aligned}
$$

The measurement probability, $p(\mathbf{z}_k|\mathbf{x}_k)$ is added because the state has to be inferred from the measurement data. Details of the derivation are presented in Appendix C.

III. INTENT INFERENCE MODELS

The belief for each case has been modeled in a probabilistic manner, and the probability distributions associated with the belief need to be defined. Both parametric and nonparametric models are used to represent the probability distributions considering their definition and properties. The modeling and evaluation procedures are described in the following.

A. PARAMETRIC MODELING

A graphical representation of the coordinate system between the own ship and the obstacle ship is shown in Fig. 3. The state $\mathbf{x}_k$ is expressed as

$$\mathbf{x}_k = \begin{bmatrix} x_{\mathrm{T},k} & y_{\mathrm{T},k} & \psi_{\mathrm{T},k} & V_{\mathrm{T},k} \end{bmatrix}^\top , \qquad (9)$$

where $x_{\mathrm{T},k}$ and $y_{\mathrm{T},k}$ represent the position of the obstacle ship at time k in the north-east-down (NED). $\psi_{\mathrm{T},k}$ and $V_{\mathrm{T},k}$ are the course and speed of the obstacle ship, respectively. The action of the obstacle ship is expressed as

$$\mathbf{u}_k = \begin{bmatrix} \omega_{\mathrm{T},k} & a_{\mathrm{T},k} \end{bmatrix}^\top , \qquad (10)$$

where $\omega_{\mathrm{T},k}$ and $a_{\mathrm{T},k}$ are the rate of turn and linear acceleration, respectively. The marine radar provides the position information in polar coordinates, and the measurement $\mathbf{z}_k$ is expressed as

$$\mathbf{z}_k = \begin{bmatrix} r_k & \beta_k \end{bmatrix}^\top , \qquad (11)$$

where r_k and β_k are relative range and bearing. The measurement probability is designed using the Gaussian distribution and is expressed as

$$p(\mathbf{z}_k|\mathbf{x}_k) \sim \mathcal{N}(\mathbf{z}_k; h(\mathbf{x}_k), R_k) , \qquad (12)$$

where $\mathcal{N}(\cdot)$ is the Gaussian distribution with the covariance R_k and the mean $h(\mathbf{x}_k)$. $h(\mathbf{x}_k)$ represents the measurement function defined by the relative position δx_k and δy_k (see Fig. 3), which is expressed as

$$h(\mathbf{x}_k) = \begin{bmatrix} \sqrt{\delta x_k^2 + \delta y_k^2} \\ \tan^{-1}(\delta y_k / \delta x_k) \end{bmatrix} . \qquad (13)$$

The state transition probability with Gaussian white noise is expressed as

$$p(\mathbf{x}_k|\mathbf{u}_k, \mathbf{x}_{k-1}) \sim \mathcal{N}(\mathbf{x}_k; f(\mathbf{x}_{k-1}, \mathbf{u}_k), Q_k) , \qquad (14)$$

where Q_k is the covariance of the process noise. The process model $f(\mathbf{x}_{k-1}, \mathbf{u}_k)$ is written as

$$
\begin{aligned}
&f(\mathbf{x}_{k-1}, \mathbf{u}_k) \\
&= \begin{bmatrix} x_{\mathrm{T},k-1} + V_{\mathrm{T},k-1} \cos\psi_{\mathrm{T},k-1} \Delta t \\ y_{\mathrm{T},k-1} + V_{\mathrm{T},k-1} \sin\psi_{\mathrm{T},k-1} \Delta t \\ \psi_{\mathrm{T},k-1} \\ V_{\mathrm{T},k-1} \end{bmatrix} + \begin{bmatrix} 0 \\ 0 \\ \omega_{\mathrm{T},k} \Delta t \\ a_{\mathrm{T},k} \Delta t \end{bmatrix} , \qquad (15)
\end{aligned}
$$

where Δt is the time difference between each step.

The intent transition probability $p(I_k|I_{k-1})$ is modeled as a transition probability matrix which is written as

$$p(I_k|I_{k-1}) = \begin{cases} p_\alpha, & \text{if } I_k = I_{k-1} \\ 1 - p_\alpha, & \text{otherwise,} \end{cases} \qquad (16)$$

where p_α represents the probability of maintaining the intention, which is assumed to be independent of time.

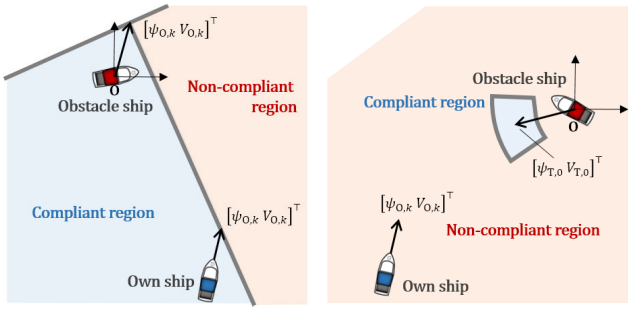

(a) Give-way for the obstacle ship (b) Stand-on for the obstacle ship

FIGURE 4. Illustrations of compliant and non-compliant velocities for the obstacle ship according to rules 16 and 17: The blue ship is the own ship and the red ship is the obstacle ship. The main coordinate system is defined as the velocity coordinate system of the obstacle ship.

B. NONPARAMETRIC MODELING

The conditional probability $p(\mathbf{u}_k|I_k, \mathbf{x}_{k-1})$ represents the probability distribution of the action to take given the previous state and the intention. The compliant and non-compliant velocity regions in the velocity coordinates centered at the location of the obstacle ship according to COLREG rules 16 and 17 are depicted in Fig. 4. Figure 4(a) shows the case when the obstacle ship is the give-way ship and Fig. 4(b) shows the case when the obstacle ship is the stand-on ship. The red region represents the non-compliant velocity of the obstacle ship, whereas the blue region represents the compliant velocity. For the give-way situation shown in Fig. 4(a), if the velocity of the obstacle ship is inside the blue region, the ship is following the rules by passing port-to-port; however, if the velocity is inside the red region, the ship is violating the rules by passing starboard-to-starboard. For the stand-on situation shown in Fig. 4(b), if the ship's velocity is inside the blue region, it means that the ship maintains its speed and course within a certain range and complies with the rules as the stand-on ship; otherwise, the obstacle ship is violating the rules. It is not straightforward to represent the probability of intention-reflected action using a parametric model. Therefore, the distribution is modeled using a nonparametric model with particles, which is expressed as

$$p(\mathbf{u}_k|I_k, \mathbf{x}_{k-1}) \approx \sum_{m=1}^{M} \frac{1}{M} \delta\left(\mathbf{u}_k - \mathbf{u}_{I,k}^{[m]}\right), \tag{17}$$

where M is the number of particles. $\mathbf{u}_{I,k}^{[m]}$ describes the m-th sampled particle of action with intention I at step k, and $\delta(\cdot)$ is the Dirac delta function [17].

The procedures for obtaining $\mathbf{u}_{I,k}^{[m]}$ are described in Fig. 5. It includes 3 steps: sampling of the non-compliant and compliant velocities, calculation of the difference in speed and course, and a sample-based approximation of the probability of intention. The leftmost figure in Fig. 5 shows the particles of the intention-reflected velocity $\mathbf{v}_{d,k} = \left[\psi_{d,k}\ V_{d,k}\right]^\top$ with respect to the region in Fig. 4. The coordinate transformation from the Cartesian coordinates to the polar coordinates is applied to the sampled velocity to calculate the difference, and is expressed as $\Delta\mathbf{v}_{d,k} = \mathbf{v}_{d,k} - \left[\psi_{T,k}\ V_{T,k}\right]^\top$. The ship takes action to reduce $\Delta\mathbf{v}_{d,k}$ to reflect the intention whose intensity depends on the decreasing rate of $\Delta\mathbf{v}_{d,k}$. The assertion of intention, which is defined as a degree of how much intention can be reflected, is inversely proportional to the time it takes for the velocity to reach $\mathbf{v}_{d,k}$. Therefore, the time is inversely proportional to the magnitude of the action, and the reflection of intention is proportional to the magnitude of the action. The rightmost figure in Fig. 5 shows the particles of the action $\mathbf{u}_k^{[m]}$ whose magnitude is proportional to the probability, and the action is bounded using its maximum and minimum values owing to the constraints of its dynamics.

If the states of the ship are satisfied with the operator's intentions, then the operator may not take any action. Therefore, no action indicates that the purpose has already been achieved. To reflect this fact, some particles of intention-reflected action which the obstacle ship has at the previous step are converted to zero action $\mathbf{u} = \left[0\ 0\right]^\top$.

C. BELIEF EVALUATION

The evaluation procedures of the three belief models with different information availability and their algorithm implementations are described.

Algorithm 1 shows the evaluation method when actions, states and measurements are all available. In line 2 of Algorithm 1, $bel(I_k^c)$ is equal to $1 - bel(I_k)$, where superscript c represents the complement set of the event. η_k in line 7 of Algorithm 1 is the normalizer which is obtained by

$$\eta_k = 1/(\mathcal{L}_{I_k,k}\overline{bel}(I_k) + \mathcal{L}_{I_k^c,k}\overline{bel}(I_k^c)). \tag{18}$$

To calculate η_k, the likelihood and prior of all intentions are calculated first. The likelihood $\mathcal{L}$ is calculated by the summation of the probability density of sampled action $\mathbf{u}_{I,k}^{[m]}$ obtained from the modeled distribution with the mean and covariance of action, $\mu_{\mathbf{u},k}$ and $\Sigma_{\mathbf{u},k}$.

Secondly, Algorithm 2 describes the belief evaluation when only the state information is available. To compensate for the lack of action information, the likelihood is calculated by accumulating the probability density of the state.

Algorithm 1 Belief Evaluation for Case 1

Input: Mean and covariance of action $\mu_{\mathbf{u},k}$, $\Sigma_{\mathbf{u},k}$, Belief of previous intention $bel(I_{k-1})$, Intent transition probability p_α, Previous state μ_{k-1}

Output: Belief of intention $bel(I_k)$

Procedure:

1: $\mathcal{L}_{I,k} = 0$
2: $\overline{bel}(I_k) \leftarrow p_\alpha bel(I_{k-1}) + (1 - p_\alpha)bel(I_{k-1}^c)$
3: **for** $m = 1$ *to* M **do**
4: Sample $\mathbf{u}_{I,k}^{[m]} \sim p(\mathbf{u}_k|I_k, \mu_{k-1})$
5: $\mathcal{L}_{I,k} \leftarrow \mathcal{L}_{I,k} + \mathcal{N}(\mathbf{u}_{I,k}^{[m]}; \mu_{\mathbf{u},k}, \Sigma_{\mathbf{u},k})$
6: **end for**
7: $bel(I_k) \leftarrow \eta_k \mathcal{L}_{I,k}\overline{bel}(I_k)$

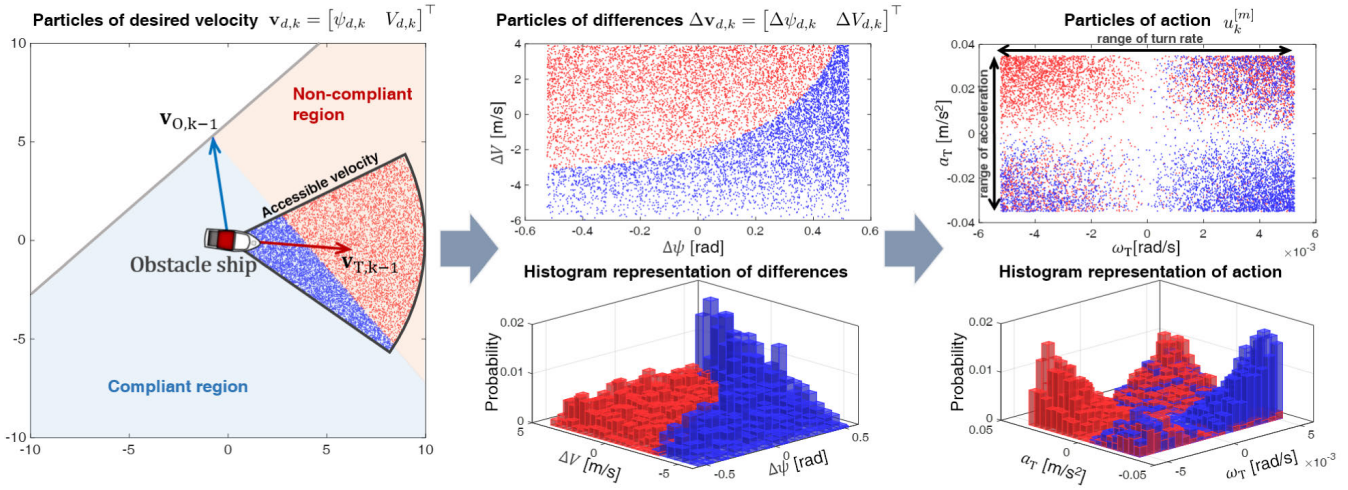

FIGURE 5. Sample-based approximation of the intention-reflected action model: The leftmost image shows the compliant and non-compliant regions in the velocity coordinates and the particles uniformly distributed in the accessible velocity area. The center image shows the particle distribution in the coordinates of speed and course changes (upper part) and its histogram representation (lower part). The rightmost image shows the corresponding plots of the particles in terms of control input $\mathbf{u}_{I,k}^{[m]}$ (yaw rate and acceleration). Red dots represent samples of non-compliant cases, whereas blue dots represent the samples of compliant cases. The state of the obstacle ship is $[-14.47 \ -323.37 \ 1.65 \ 6.09]^\top$ and that of the own ship is $[-335.24 \ -13.84 \ 6.14 \ 5.33]^\top$.

Algorithm 2 Belief Evaluation for Case 2

Input: Mean and covariance of state μ_k, Σ_k, Covariance of process noise Q_k, Belief of previous intention $bel(I_{k-1})$, Intent transition probability p_α, Mean and covariance of previous state μ_{k-1}, Σ_{k-1}

Output: Belief of intention $bel(I_k)$

Procedure:

$\mathcal{L}_{I,k} = 0$
$\overline{bel}(I_k) \leftarrow p_\alpha bel(I_{k-1}) + (1 - p_\alpha) bel(I_{k-1}^c)$
for $m = 1$ *to* M **do**
  Sample $\mathbf{x}_{k-1}^{[m]} \sim \mathcal{N}(\mathbf{x}_{k-1}; \mu_{k-1}, \Sigma_{k-1})$
  Sample $\mathbf{u}_{I,k}^{[m]} \sim p(\mathbf{u}_k | I_k, \mathbf{x}_{k-1}^{[m]})$
  Sample $\mathbf{x}_{I,k}^{[m]} \sim \mathcal{N}(\mathbf{x}_k; f(\mathbf{x}_{k-1}, \mathbf{u}_{I,k}^{[m]}), Q_k)$
  $\mathcal{L}_{I,k} \leftarrow \mathcal{L}_{I,k} + \mathcal{N}(\mathbf{x}_{I,k}^{[m]}; \mu_k, \Sigma_k)$
end for
$bel(I_k) \leftarrow \eta_k \mathcal{L}_{I,k} \overline{bel}(I_k)$

Finally, Algorithm 3 shows the evaluation of the belief when only measurements are available. To calculate the belief efficiently with a smaller number of particles, the probability of the intention-reflected state $p(\mathbf{x}_k | I_k, \mathbf{z}_{1:k})$ is approximated using a Gaussian distribution. $p(\mathbf{x}_k | I_k, \mathbf{z}_{1:k})$ is updated from $p(\mathbf{x}_k | I_k, \mathbf{z}_{1:k-1})$ using an extended Kalman filter to avoid particle deprivation. As a result, the probability of the state is represented by a Gaussian mixture model (GMM) with weights $bel(I_k)$, which is expressed as

$$p(\mathbf{x}_k | \mathbf{z}_{1:k}) = \sum_{I_k} p(I_k | \mathbf{z}_{1:k}) p(\mathbf{x}_k | I_k, \mathbf{z}_{1:k}) = \sum_{I_k} bel(I_k) p(\mathbf{x}_k | I_k, \mathbf{z}_{1:k}). \quad (19)$$

Algorithm 3 Belief Evaluation for Case 3

Input: Measurement $\mathbf{z}_k$, Covariance of process and measurement noise Q_k, R_k, Previous GMM $p(\mathbf{x}_{k-1} | \mathbf{z}_{1:k-1})$, Intent transition probability p_α

Output: Belief of intention $bel(I_k)$

Procedure:

for $m = 1$ *to* M **do**
  Sample $\mathbf{x}_{k-1}^{[m]} \sim p(\mathbf{x}_{k-1} | I_{k-1}, \mathbf{z}_{1:k-1})$
  Sample $\mathbf{u}_{I,k}^{[m]} \sim p(\mathbf{u}_k | I_k, \mathbf{x}_{k-1}^{[m]})$
  Sample $\mathbf{x}_{I,k}^{[m]} \sim \mathcal{N}(\mathbf{x}_k; f(\mathbf{x}_{k-1}^{[m]}, \mathbf{u}_{I,k}^{[m]}), Q_k)$
  $w_{I,k}^{[m]} \leftarrow \mathcal{N}(\mathbf{z}_k; h(\mathbf{x}_{I,k}^{[m]}), R_k) p_\alpha bel(I_{k-1})$
end for
for $m = M + 1$ *to* $2M$ **do**
  Sample $\mathbf{x}_{k-1}^{[m]} \sim p(\mathbf{x}_{k-1} | I_{k-1}^c, \mathbf{z}_{1:k-1})$
  Sample $\mathbf{u}_{I,k}^{[m]} \sim p(\mathbf{u}_k | I_k, \mathbf{x}_{k-1}^{[m]})$
  Sample $\mathbf{x}_{I,k}^{[m]} \sim \mathcal{N}(\mathbf{x}_k; f(\mathbf{x}_{k-1}^{[m]}, \mathbf{u}_{I,k}^{[m]}), Q_k)$
  $w_{I,k}^{[m]} \leftarrow \mathcal{N}(\mathbf{z}_k; h(\mathbf{x}_{I,k}^{[m]}), R_k)(1 - p_\alpha) bel(I_{k-1}^c)$
end for
$bel(I_k) = \eta_k \sum_{m=1}^{2M} w_{I,k}^{[m]}$

IV. SIMULATION FOR VALIDATION

A. SIMULATION SETTING

The scenario settings of the traffic simulations for evaluating the performance of the proposed intent-inference method is depicted in Fig. 6. Two ships, an observing ship and an obstacle ship observed by the observing ship, cross each other. The observing ship gathers information on the obstacle ship and predicts its intention using the gathered information.

TABLE 1. Parameter settings for performance test of the algorithm.

variables		value	unit
Accessible velocity	yaw	$[\psi_{\mathrm{T}} - 30.0, \psi_{\mathrm{T}} + 30.0]$	deg
	speed	$[0.0, 10.0]$	m
Accessible action	turn rate	$[-0.3, 0.3]$	deg/s
	acceleration	$[-0.035, 0.035]$	m/s^2
Noise of marine radar	range	$\mathcal{U}(-74.9, 74.9)^*$	m
	bearing	$\mathcal{U}(-0.475, 0.475)$	deg
Noise of AIS	x-position	$\mathcal{N}(0, 0.5^2 + v_{x\mathrm{T}}^2/12)^{*,**}$	m
	y-position	$\mathcal{N}(0, 0.5^2 + v_{y\mathrm{T}}^2/12)^{**}$	m
	x-velocity	$\mathcal{N}(0, 0.1^2)$	m/s
	y-velocity	$\mathcal{N}(0, 0.1^2)$	m/s
The number of particles (M)		5000	-
The number of simulation		400	-

* $\mathcal{U}$: uniform distribution, $\mathcal{N}$: Gaussian distribution
** $v_{x\mathrm{T}} = V_{\mathrm{T}} \cos\psi_{\mathrm{T}}$, $v_{y\mathrm{T}} = V_{\mathrm{T}} \sin\psi_{\mathrm{T}}$

The obstacle ship is set to randomly perform either a compliant or non-compliant maneuver against the observing ship. When the obstacle ship has an obligation to maintain its course and speed, it maintains its course and speed if it intends to comply with the rule; however, it alters its course to a randomly biased course if it intends to violate the rule. According to the rule, if the obstacle ship needs to avoid the other ship, then non-compliant intention makes the evasive maneuver on the port side, whereas the compliant intention makes the evasive maneuver on the starboard side.

In every simulation run, two ships appear simultaneously from two randomly chosen points among eight starting points, and then they cross each other as shown in Fig. 6. To make a sufficiently close encounter in every single scenario, both the ships approach the center point of the simulation field with a randomly biased course and speed. The size of the simulation field is a square 10 nautical miles (nmi) long on one side. The length and breadth of the ship are 175 m and 25.4 m, respectively. The mathematical model of a container ship is used for dynamic simulations, and the detailed model information is available in [18], [19]. The transition probability of the intention, p_α, is set to 0.95. The frequency of the sensor measurement, and its inference is set to 0.1 Hz.

The information of AIS and marine radar is calculated by adding noise components to the true data. The noise of the AIS is modeled using the Gaussian distribution [20], and the noise of the marine radar in range and bearing is modeled using the uniform distribution. Four-hundred random-encounter traffic simulations were conducted for the three cases of observation settings defined in Section II-C. In the first case, the observing ship obtains all the necessary information without noise. In the second case, the observing ship uses the noisy state information of the obstacle ship. Finally, in the third case, the observing ship uses only the noisy measurement of the obstacle ship. The details of the simulation setting are shown in the Table 1.

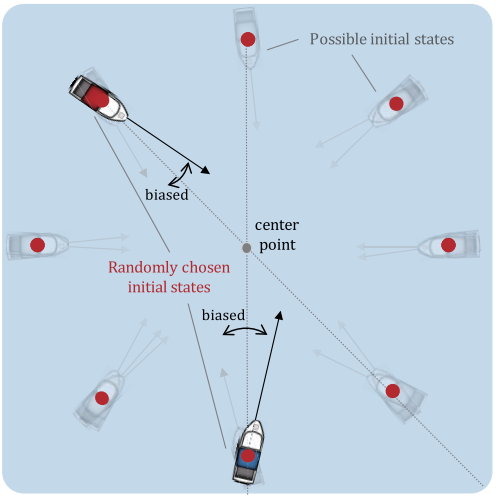

FIGURE 6. A graphical representation of the simulation setting. The own ship and the obstacle ship are set to randomly appear from 8 possible different directions.

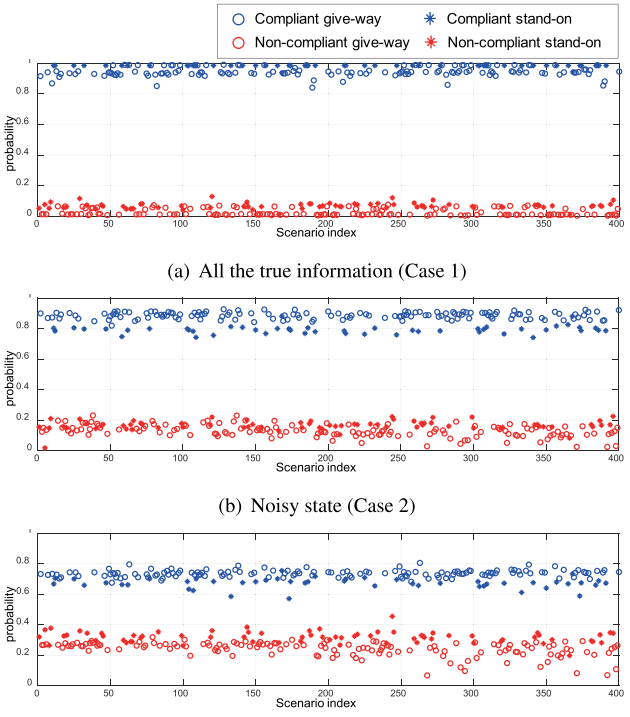

(a) All the true information (Case 1)

(b) Noisy state (Case 2)

(c) Noisy measurement (Case 3)

FIGURE 7. Average probability of compliant intention. The blue represents the scenario with compliant intention, while the red represents the scenario with non-compliant intention. Circles and asterisks represent encounters with give-way and stand-on obligations, respectively.

B. RESULT AND DISCUSSION

The result of estimating intention using the proposed algorithm through the Monte-Carlo simulation for the three cases of observation settings is shown in Fig. 7. The x-axis of each graph is the index of the scenario, and the y-axis is the estimated probability of compliant intention. In the resulting graph, a blue represents the case with the com-

TABLE 2. Quantitative performance of intent inference result according to the distance between the two ships.

		Detection distance: 3.0 nmi			Detection distance: 4.5 nmi			Detection distance: 10 nmi		
Margin (p_m)	Algorithm	Precision	Recall	F_1 score	Precision	Recall	F_1 score	Precision	Recall	F_1 score
0.00	Case 1	**1.0000**	**1.0000**	**1.0000**	**0.9991**	**0.9991**	**0.9991**	**0.9673**	**0.9673**	**0.9673**
	Case 2	0.9996	0.9996	0.9996	0.9987	0.9987	0.9987	0.9616	0.9616	0.9616
	Case 3	0.9580	0.9580	0.9580	0.9434	0.9434	0.9434	0.8914	0.8914	0.8914
0.05	Case 1	**1.0000**	**1.0000**	**1.0000**	**0.9991**	**0.9991**	**0.9991**	**0.9679**	**0.9665**	**0.9672**
	Case 2	0.9999	0.9996	0.9990	0.9991	0.9975	0.9983	0.9641	0.9525	0.9583
	Case 3	0.9996	0.9983	0.9990	0.9591	0.9064	0.9320	0.9273	0.8299	0.8759
0.10	Case 1	**1.0000**	**1.0000**	**1.0000**	0.9990	**0.9990**	**0.9990**	0.9682	**0.9655**	**0.9668**
	Case 2	0.9999	0.9965	0.9982	**0.9994**	0.9952	0.9973	**0.9707**	0.9446	0.9575
	Case 3	0.9803	0.8912	0.9336	0.9736	0.8639	0.9154	0.9525	0.7717	0.8526
0.15	Case 1	**1.0000**	**1.0000**	**1.0000**	0.9990	**0.9990**	**0.9990**	0.9690	**0.9647**	**0.9669**
	Case 2	**1.0000**	0.9917	0.9958	**0.9995**	0.9902	0.9948	**0.9773**	0.9338	0.9551
	Case 3	0.9880	0.8421	0.9092	0.9840	0.8028	0.8842	0.9714	0.6973	0.8118

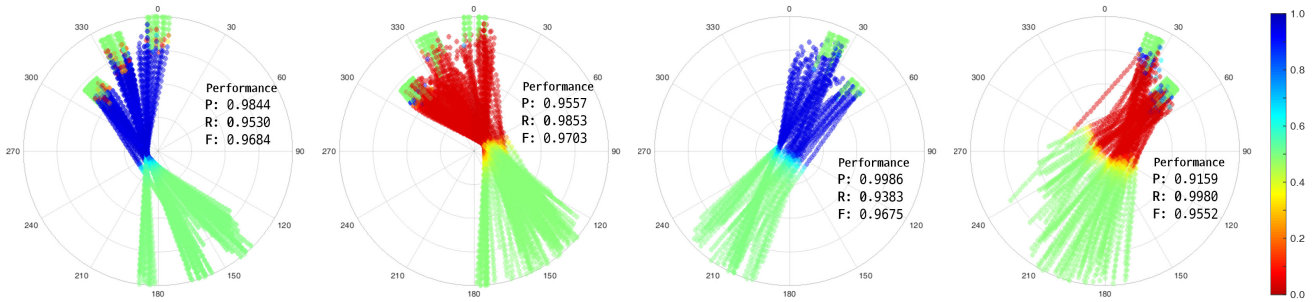

(a) Compliant give-way situation (b) Non-compliant give-way situation (c) Compliant stand-on situation (d) Non-compliant stand-on situation

FIGURE 8. Belief of compliant intention in each scenario (Case 1). Circles are the relative positions in the body-fixed coordinates of the observing ship. The color of the circles represents the belief of intention. The radius of the polar coordinates is 10.0 nmi. (P: precision, R: recall, F: F_1 score).

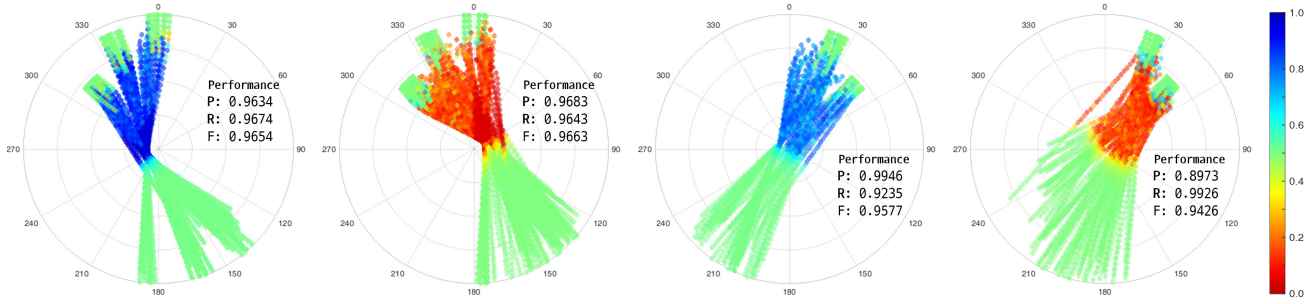

(a) Compliant give-way situation (b) Non-compliant give-way situation (c) Compliant stand-on situation (d) Non-compliant stand-on situation

FIGURE 9. Belief of compliant intention in each scenario (Case 2). Circles are the relative positions in the body-fixed coordinates of the observing ship. The color of the circles represents the belief of intention. The radius of the polar coordinates is 10.0 nmi. (P: precision, R: recall, F: F_1 score).

pliant intention, while a red represents the case with the non-compliant intention. Therefore, the blue has a higher probability, whereas the red has a lower probability. This further indicates that the intentions are properly estimated by the proposed algorithm. In particular, the more reliable information provided, the more clearly the intention can be distinguished.

The result of trajectory and belief are depicted in Figs. 8, 9, and 10. The circle represents the position of the obstacle ship in the body-fixed frame of the observing ship during every minute. The heading angle of the observing ship points upward in the coordinate system. The first two figures (from the left) in each of the cases show the result of the give-way situation of the obstacle ship, and thus the obstacle

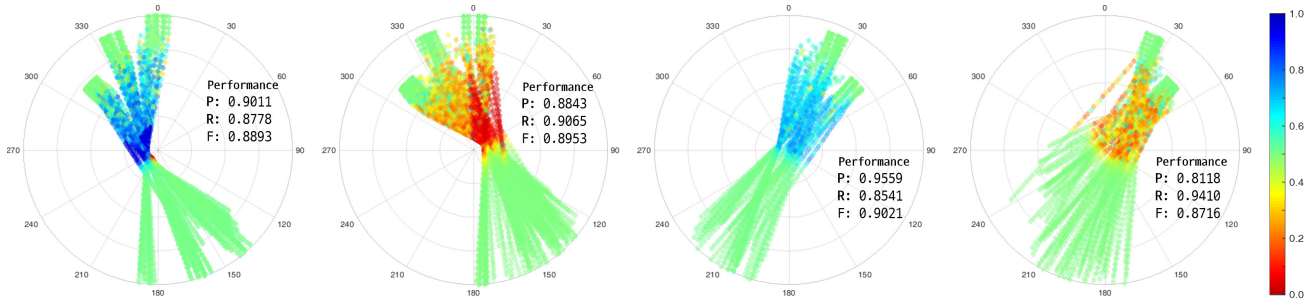

(a) Compliant give-way situation (b) Non-compliant give-way situation (c) Compliant stand-on situation (d) Non-compliant stand-on situation

FIGURE 10. Belief of compliant intention in each scenario (Case 3). Circles are the relative positions in the body-fixed coordinates of the observing ship. The color of the circles represents the belief of intention. The radius of the polar coordinates is 10.0 nmi. (P: precision, R: recall, F: F_1 score).

ship approaches from the bow port side of the observing ship. Meanwhile, the other figures in each case show the results of the stand-on situation of the obstacle ship, and thus the obstacle ship approaches from the starboard side. The obstacle ship avoids the observing ship by turning to the stern of the observing ship in the give-way situation with compliant intention (see first column), whereas it avoids the observing ship by turning to the bow of the observing ship in the give-way situation with non-compliant intention (see second column).

The color of the circles represents the belief of compliant intention. The red, blue, and green represent the violation, compliance, and neutrality, respectively. In the situations with compliant intentions, most of the circles are blue. Meanwhile, most circles are red in non-compliant situations. The resultant color of the circle indicates that the inference is performed correctly. In particular, the closer the obstacle ship is to the observing ship, the more accurate the inferred maneuver intention is.

Table 2 summarizes the quantitative results for precision, recall, and F_1 score depending on the detection distance. The inferred probability value is approximately 0.5, and this indicates that the intent inference algorithm may not clearly distinguish the intention. Therefore, a neutral range is predefined and the intention is estimated outside the neutral zone with a width of $2p_m$. The inferred intention that varies with the width of the neutral zone is expressed as

$$\text{Intent} = \begin{cases} \text{Compliant}, & \text{if } bel(I_k = \mathcal{C}) > 0.5 + p_m \\ \text{Non-compliant}, & \text{if } bel(I_k = \mathcal{V}) > 0.5 + p_m \\ \text{Neutral}, & \text{otherwise.} \end{cases} \tag{20}$$

The precision is the fraction of the correct answers among the estimation of the algorithm, whereas the recall is the fraction of the correct answers with respect to the corresponding situations. As the value of the threshold increases, the compliance or violation is more carefully estimated. Therefore, because the algorithm gives the answer "neutral" more frequently in the ambiguous situations, the recall decreases, whereas the precision increases. The more accurate and reliable the information is, the higher the F_1 score is. Figures 8, 9, and 10 show that the intention is not clearly identified at far distance where evasive actions are not taken yet; however, the performance of intent inference improves as the two ships get closer. The quantitative performance is evaluated at varying distances. Note that 4.5 nmi is the range where the collision risk exists according to the case law [21], and 3.0 nmi is the minimum range of the onboard lights in rule 22 of the COLREGs. The computational efficiency of the proposed algorithm was confirmed to be very satisfactory. The update rate higher than 5 Hz was obtained using MATALB and an even higher rate can be achieved by optimizing the algorithm software and the hardware system, which is fast enough for ship applications.

V. CONCLUSION

This study proposes a systematic procedure for estimating the maneuver intention of an encountered ship to predict its compliance/violation of COLREGs. The main contribution of this paper is summarized as follows:

- The DBN-based graphical model which represents the relationship between the intention and observations of traffic ships was constructed, and the conditional independence between the variables in the graphical model was determined.
- The probability distribution associated with the graphical model was factorized using the probabilistic tools and evaluated using the parametric and nonparametric methods. Then, the systematic intent inference procedure was designed and implemented for three different cases of information availability.
- Monte-Carlo-based ship-encounter simulations were performed and their results were analyzed in order to verify the performance of the proposed approach. The results confirmed that the proposed intent inference method can achieve a satisfactory accuracy even with a limited amount of trajectory information of obstacle ships, such as noise-corrupted range and bearing measurements provided by marine radar.

APPENDIX MATHEMATICAL DERIVATION OF THE BELIEF OF INTENT

A. DERIVATION OF EQUATION 3

Here, the details of mathematical derivation of (3) are presented. The first process of the derivation involves application of the Bayes' rule to (2):

$$\begin{aligned} &p(I_k|\mathbf{u}_{1:k}, \mathbf{x}_{0:k-1}) \\ &\quad = \frac{p(\mathbf{u}_k|I_k, \mathbf{u}_{1:k-1}, \mathbf{x}_{0:k-1})p(I_k|\mathbf{u}_{1:k-1}, \mathbf{x}_{0:k-1})}{p(\mathbf{u}_k|\mathbf{u}_{1:k-1}, \mathbf{x}_{0:k-1})} \\ &\quad = \eta_k p(\mathbf{u}_k|I_k, \mathbf{u}_{1:k-1}, \mathbf{x}_{0:k-1})p(I_k|\mathbf{u}_{1:k-1}, \mathbf{x}_{0:k-1}), \end{aligned} \tag{21}$$

where η_k is used as a normalizer. The intention is described as a discrete random variable and $p(I_k|\mathbf{u}_{1:k-1}, \mathbf{x}_{0:k-1})$ can be expanded using the law of total probability:

$$\begin{aligned} &p(I_k|\mathbf{u}_{1:k-1}, \mathbf{x}_{0:k-1}) \\ &\quad = \sum_{I_{k-1}} p(I_k|I_{k-1}, \mathbf{u}_{1:k-1}, \mathbf{x}_{0:k-1})p(I_{k-1}|\mathbf{u}_{1:k-1}, \mathbf{x}_{0:k-1}). \end{aligned} \tag{22}$$

In order to reduce the equations to ones with only the meaningful variables, the conditional independence is checked using d-separation. $\mathbf{u}_k$ is conditionally independent of $\mathbf{u}_{1:k-1}$ and $\mathbf{x}_{0:k-2}$ given $I_k, \mathbf{x}_{k-1}$ in (21):

$$p(\mathbf{u}_k|I_k, \mathbf{u}_{1:k-1}, \mathbf{x}_{0:k-1}) = p(\mathbf{u}_k|I_k, \mathbf{x}_{k-1}). \tag{23}$$

In (22), I_k is conditionally independent of $\mathbf{u}_{1:k-1}$ and $\mathbf{x}_{0:k-1}$ given I_{k-1}. Also, I_{k-1} is conditionally independent of $\mathbf{x}_{k-1}$ given $\mathbf{u}_{1:k-1}, \mathbf{x}_{0:k-2}$. Above conditional independence of the probability distribution can be written as

$$\begin{aligned} p(I_k|I_{k-1}, \mathbf{u}_{1:k-1}, \mathbf{x}_{0:k-1}) &= p(I_k|I_{k-1}) \\ p(I_{k-1}|\mathbf{u}_{1:k-1}, \mathbf{x}_{0:k-1}) &= p(I_{k-1}|\mathbf{u}_{1:k-1}, \mathbf{x}_{0:k-2}). \end{aligned} \tag{24}$$

By applying (24) to (22), and then (22) and (23) to (21), (3) is obtained.

B. DERIVATION OF EQUATION 5

The law of total probability is firstly applied for the derivation of (5):

$$p(I_k|\mathbf{x}_{0:k}) = \int_{\mathbf{u}_k} p(I_k, \mathbf{u}_k|\mathbf{x}_{0:k})d\mathbf{u}_k, \tag{25}$$

where $\mathbf{u}_k$ is a continuous random variable. Above equation is expanded using the Bayes' rule:

$$\begin{aligned} &\int_{\mathbf{u}_k} p(I_k, \mathbf{u}_k|\mathbf{x}_{0:k})d\mathbf{u}_k \\ &\quad = \int_{\mathbf{u}_k} \frac{p(\mathbf{x}_k|I_k, \mathbf{u}_k, \mathbf{x}_{0:k-1})p(I_k, \mathbf{u}_k|\mathbf{x}_{0:k-1})}{p(\mathbf{x}_k|\mathbf{x}_{0:k-1})}d\mathbf{u}_k \\ &\quad = \eta_k \int_{\mathbf{u}_k} p(\mathbf{x}_k|I_k, \mathbf{u}_k, \mathbf{x}_{0:k-1})p(I_k, \mathbf{u}_k|\mathbf{x}_{0:k-1})d\mathbf{u}_k, \end{aligned} \tag{26}$$

where η_k is constant with respect to the $\mathbf{u}_k$. Using a conditional probability, the joint probability of intention and action is expanded as

$$p(I_k, \mathbf{u}_k|\mathbf{x}_{0:k-1}) = p(\mathbf{u}_k|I_k, \mathbf{x}_{0:k-1})p(I_k|\mathbf{x}_{0:k-1}). \tag{27}$$

Once again, $p(I_k|\mathbf{x}_{0:k-1})$ is expanded using the law of total probability as follow:

$$p(I_k|\mathbf{x}_{0:k-1}) = \sum_{I_{k-1}} p(I_k|I_{k-1}, \mathbf{x}_{0:k-1})p(I_{k-1}|\mathbf{x}_{0:k-1}). \tag{28}$$

In (26), $\mathbf{x}_k$ is conditionally independent of I_k, $\mathbf{x}_{0:k-2}$ given $\mathbf{x}_{k-1}, \mathbf{u}_k$, and the resulting equation can be simplified into

$$p(\mathbf{x}_k|I_k, \mathbf{u}_k, \mathbf{x}_{0:k-1}) = p(\mathbf{x}_k|\mathbf{u}_k, \mathbf{x}_{k-1}). \tag{29}$$

The probability of action in (27) is simplified using d-separation as follows:

$$p(\mathbf{u}_k|I_k, \mathbf{x}_{0:k-1}) = p(\mathbf{u}_k|I_k, \mathbf{x}_{k-1}), \tag{30}$$

where $\mathbf{u}_k$ is conditionally independent of $\mathbf{x}_{0:k-2}$ given I_k, $\mathbf{x}_{k-1}$. Also, the probability of intention in (28) is simplified using d-separation as follow:

$$p(I_k|I_{k-1}, \mathbf{x}_{0:k-1}) = p(I_k|I_{k-1}), \tag{31}$$

where I_k is conditionally independent of $\mathbf{x}_{0:k-1}$ given I_{k-1}. All substitutions of (27) and (28) and simplification of (29), (30), and (31) are applied to (26) yielding (5).

C. DERIVATION OF EQUATION 8

The first step of mathematical derivation includes Bayes' rule to (8):

$$\begin{aligned} p(\mathbf{x}_k, I_k|\mathbf{z}_{1:k}) &= \frac{p(\mathbf{z}_k|\mathbf{x}_k, I_k, \mathbf{z}_{1:k-1})p(\mathbf{x}_k, I_k|\mathbf{z}_{1:k-1})}{p(\mathbf{z}_k|\mathbf{z}_{1:k-1})} \\ &= \eta_k p(\mathbf{z}_k|\mathbf{x}_k, I_k, \mathbf{z}_{1:k-1})p(\mathbf{x}_k, I_k|\mathbf{z}_{1:k-1}). \end{aligned} \tag{32}$$

Since $\mathbf{z}_k$ is conditionally independent of I_k and $\mathbf{z}_{1:k-1}$ given $\mathbf{x}_k$, the above equation can be rewritten as

$$\eta_k p(\mathbf{z}_k|\mathbf{x}_k)p(\mathbf{x}_k, I_k|\mathbf{z}_{1:k-1}). \tag{33}$$

The joint probability of state and intention is expanded using the law of total probability as follows:

$$\begin{aligned} &p(\mathbf{x}_k, I_k|\mathbf{z}_{1:k-1}) \\ &\quad = \iint_{\mathbf{x}_{k-1}, \mathbf{u}_k} p(\mathbf{x}_k, I_k, \mathbf{x}_{k-1}, \mathbf{u}_k|\mathbf{z}_{1:k-1})d\mathbf{u}_k d\mathbf{x}_{k-1}. \end{aligned} \tag{34}$$

The joint probability inside the integral sign is equal to the product of three probabilities by the chain rule:

$$\begin{aligned} &p(\mathbf{x}_k, I_k, \mathbf{x}_{k-1}, \mathbf{u}_k|\mathbf{z}_{1:k-1}) \\ &\quad = p(\mathbf{x}_k|\mathbf{u}_k, \mathbf{x}_{k-1}, I_k, \mathbf{z}_{1:k-1}) \\ &\qquad p(\mathbf{u}_k|\mathbf{x}_{k-1}, I_k, \mathbf{z}_{1:k-1})p(\mathbf{x}_{k-1}, I_k|\mathbf{z}_{1:k-1}). \end{aligned} \tag{35}$$

By d-separation, the probability of state and the probability of action can be written as

$$\begin{aligned} p(\mathbf{x}_k|\mathbf{u}_k, \mathbf{x}_{k-1}, I_k, \mathbf{z}_{1:k-1}) &= p(\mathbf{x}_k|\mathbf{u}_k, \mathbf{x}_{k-1}) \\ p(\mathbf{u}_k|\mathbf{x}_{k-1}, I_k, \mathbf{z}_{1:k-1}) &= p(\mathbf{u}_k|\mathbf{x}_{k-1}, I_k). \end{aligned} \tag{36}$$

The joint probability of previous state and intention can be expanded by the law of total probability with discrete random

variable:

$$p(\mathbf{x}_{k-1}, I_k|\mathbf{z}_{1:k-1}) = \sum_{I_{k-1}} p(I_k|\mathbf{x}_{k-1}, I_{k-1}, \mathbf{z}_{1:k-1}) p(\mathbf{x}_{k-1}, I_{k-1}|\mathbf{z}_{1:k-1}) = \sum_{I_{k-1}} p(I_k|I_{k-1}) p(\mathbf{x}_{k-1}, I_{k-1}|\mathbf{z}_{1:k-1}), \quad (37)$$

where $p(I_k|\mathbf{x}_{k-1}, I_{k-1}, \mathbf{z}_{1:k-1})$ is rewritten as $p(I_k|I_{k-1})$ using d-separation. The resulting equation is equal to (8) from applying (34), (35), (36), and (37) to (33).

REFERENCES

[1] *COLREGS—International Regulations for Preventing Collisions at Sea*, Convention on the International Regulations for Preventing Collisions at Sea, 1972, IMO, London, U.K., 1972.
[2] Y. Cho, J. Han, J. Kim, P. Lee, and S.-B. Park, "Experimental validation of a velocity obstacle based collision avoidance algorithm for unmanned surface vehicles," *IFAC-PapersOnLine*, vol. 52, no. 21, pp. 329–334, 2019.
[3] J. Han, Y. Cho, J. Kim, J. Kim, N. Son, and S. Y. Kim, "Autonomous collision detection and avoidance for ARAGON USV: Development and field tests," *J. Field Robot.*, vol. 37, no. 6, pp. 987–1002, Sep. 2020.
[4] Y. Cho, J. Han, and J. Kim, "Efficient COLREG-compliant collision avoidance in multi-ship encounter situations," *IEEE Trans. Intell. Transp. Syst.*, early access, Oct. 20, 2020, doi: 10.1109/TITS.2020.3029279.
[5] Y. Cho, J. Han, and J. Kim, "Intent inference of ship maneuvering for automatic ship collision avoidance," *IFAC-PapersOnLine*, vol. 51, no. 29, pp. 384–388, 2018.
[6] J. Krozel and D. Andrisani, "Intent inference with path prediction," *J. Guid., Control, Dyn.*, vol. 29, no. 2, pp. 225–236, Mar. 2006.
[7] J. L. Yepes, I. Hwang, and M. Rotea, "New algorithms for aircraft intent inference and trajectory prediction," *J. Guid., Control, Dyn.*, vol. 30, no. 2, pp. 370–382, Mar. 2007.
[8] I. Hwang and C. Eng Seah, "Intent-based probabilistic conflict detection for the next generation air transportation system," *Proc. IEEE*, vol. 96, no. 12, pp. 2040–2059, Dec. 2008.
[9] W. Zhang, F. Yang, and Y. Liang, "A Bayesian framework for joint target tracking, classification, and intent inference," *IEEE Access*, vol. 7, pp. 66148–66156, 2019.
[10] J. W. Leavitt, "Intent-aware collision avoidance for autonomous marine vehicles," Ph.D. dissertation, Dept. Mech. Eng., Elect. Eng., Comput. Sci., Massachusetts Inst. Technol., Cambridge, MA, USA, 2017.
[11] P. Svec, B. C. Shah, I. R. Bertaska, J. Alvarez, A. J. Sinisterra, K. von Ellenrieder, M. Dhanak, and S. K. Gupta, "Dynamics-aware target following for an autonomous surface vehicle operating under COLREGs in civilian traffic," in *Proc. IEEE/RSJ Int. Conf. Intell. Robots Syst.*, Nov. 2013, pp. 3871–3878.
[12] B. C. Shah, P. Svec, I. R. Bertaska, W. Klinger, A. J. Sinisterra, K. V. Ellenrieder, M. Dhanak, and S. K. Gupta, "Trajectory planning with adaptive control primitives for autonomous surface vehicles operating in congested civilian traffic," in *Proc. IEEE/RSJ Int. Conf. Intell. Robots Syst.*, Sep. 2014, pp. 2312–2318.
[13] B. C. Shah, P. Švec, I. R. Bertaska, A. J. Sinisterra, W. Klinger, K. von Ellenrieder, M. Dhanak, and S. K. Gupta, "Resolution-adaptive risk-aware trajectory planning for surface vehicles operating in congested civilian traffic," *Auto. Robots*, vol. 40, no. 7, pp. 1139–1163, Oct. 2016.
[14] L. Du, F. Goerlandt, O. A. V. Banda, Y. Huang, Y. Wen, and P. Kujala, "Improving stand-on ship's situational awareness by estimating the intention of the give-way ship," *Ocean Eng.*, vol. 201, Apr. 2020, Art. no. 107110.
[15] K. Woerner, M. R. Benjamin, M. Novitzky, and J. J. Leonard, "Quantifying protocol evaluation for autonomous collision avoidance," *Auto. Robots*, vol. 43, no. 4, pp. 967–991, 2018.
[16] S. Thrun, W. Burgard, and D. Fox, *Probabilistic Robotics*. Cambridge, MA, USA: MIT Press, 2005.
[17] N. Gordon, B. Ristic, and S. Arulampalam, *Beyond the Kalman Filter: Particle Filters for Tracking Applications*, vol. 830, no. 5. London, U.K.: Artech House, 2004, pp. 1–4.
[18] K. Son and K. Nomoto, "On the coupled motion of steering and rolling of a high-speed container ship," *Nav. Archit. Ocean Eng.*, vol. 20, pp. 73–83, 1982.
[19] T. I. Fossen, *Handbook of Marine Craft Hydrodynamics and Motion Control*. Hoboken, NJ, USA: Wiley, 2011.
[20] T. Fossen, K. Pettersen, and H. Nijmeijer, *Sensing and Control for Autonomous Vehicles*. Cham, Switzerland: Springer, 2017.
[21] C. H. Allen, *Farwell's Rules of the Nautical Road*. Annapolis, MD, USA: US Naval Institute, 2004.

YONGHOON CHO (Graduate Student Member, IEEE) received the B.S. degree in mechanical engineering from Inha University, Incheon, South Korea, in 2014. He is currently pursuing the integrated m.s.-ph.d. degree with the Department of Mechanical Engineering, Korea Advanced Institute of Science and Technology, Daejeon, South Korea. His research interests include autonomous navigation and collision avoidance for USVs.

JONGHWI KIM (Graduate Student Member, IEEE) received the B.S. and M.S. degrees in mechanical engineering from Korea Advanced Institute of Science and Technology, Daejeon, South Korea, in 2017 and 2019, respectively, where he is currently pursuing the Ph.D. degree in mechanical engineering. His research interests include vehicle localization and sensor fusion.

JINWHAN KIM (Member, IEEE) received the B.S. and M.S. degrees in naval architecture and ocean engineering from Seoul National University, Seoul, South Korea, and the Ph.D. degree in aeronautics and astronautics from Stanford University. He has been with the Faculty of Mechanical Engineering, Korea Advanced Institute of Science and Technology, Daejeon, South Korea. He is a Senior Member of AIAA.